Crystal Structure of the Leadzyme at 1.8 Å Resolution: Metal Ion Binding and the Implications for Catalytic Mechanism and Allo Site Ion Regulation†

Joseph E. Wedekind‡,§ and David B. McKay*,‡

Department of Structural Biology, Stanford University School of Medicine, Stanford, California 94305, and Department of Biochemistry and Biophysics, University of Rochester Medical Center, Rochester, New York 14642

Received March 27, 2003

ABSTRACT: The leadzyme is a small ribozyme, derived from *in vitro* selection, which catalyzes site specific, Pb^{2+}-dependent RNA cleavage. Pb^{2+} is required for activity; Mg^{2+} inhibits activity, while many divalent and trivalent ions enhance it. The leadzyme structure consists of an RNA duplex interrupted by a trinucleotide bulge. Here, crystal structures determined to 1.8 Å resolution, both with Mg^{2+} as the sole divalent counterion and with Mg^{2+} and Sr^{2+} (which mimics Pb^{2+} with respect to binding but not catalysis), reveal the metal ion interactions with both the ground state and precatalytic conformations of the leadzyme. $Mg(H_2O)_6^{2+}$ ions bridge complementary strands of the duplex at multiple locations by binding tandem purines of one RNA strand in the major groove. At one site, $Mg(H_2O)_6^{2+}$ ligates the phosphodiester backbone of the trinucleotide bulge in the ground state conformation, but not in the precatalytic conformation, suggesting (a) Mg^{2+} may inhibit leadzyme activity by stabilizing the ground state and (b) metal ions which displace Mg^{2+} from this site may activate the leadzyme. Binding of Sr^{2+} to the presumed catalytic Pb^{2+} site in the precatalytic leadzyme induces local structural changes in a manner that would facilitate alignment of the catalytic ribose 2′-hydroxyl with the scissile bond for cleavage. These data support a model wherein binding of a catalytic ion to a precatalytic conformation of the leadzyme, in conjunction with the flexibility of the trinucleotide bulge, may facilitate structural rearrangements around the scissle phosphodiester bond favoring configurations that allow bond cleavage.

The "leadzyme" is a small ribozyme derived by *in vitro* selection for RNA sequences that exhibit site specific Pb^{2+}-dependent RNA cleavage activity (*1*, *2*). The consensus sequence motif for the leadzyme can be described as a short duplex with an internal bulge loop (Scheme 1). In the first half of a two-step reaction, the motif uses Pb^{2+} to cleave the phosphodiester backbone of the substrate strand, yielding a free 5′-hydroxyl and a 2′,3′-cyclic phosphodiester as products, which is analogous to the activity catalyzed by naturally occurring small ribozymes such as the hammerhead and hairpin. The cyclic phosphate is hydrolyzed subsequently to produce a 3′-phosphate in a manner similar to that of protein ribonuclease A; this second step is not observed in the hammerhead or hairpin ribozyme reaction. The logarithm of the cleavage rate increases linearly with pH over the range of 5.5−7.0, suggesting participation of a Pb^{2+}-coordinated hydroxide ion acting as a general base (*3*). The requirement for Pb^{2+} at concentrations on the order of ∼10 μM is obligatory, and no other metal ion has been shown to replace Pb^{2+} as a cofactor in the cleavage reaction. However, the presence of a second metal ion in addition to Pb^{2+} can enhance the cleavage rate. In particular, lanthanides enhance the reaction rate by as much as 1 order of magnitude, which led to a mechanistic proposal that two metal ions participate directly in bond cleavage (*4*, *5*). Notably, at concentrations on the order of ∼10 mM, Mg^{2+} reduces the cleavage rate, which was attributed to possible competitive inhibition with Pb^{2+} binding (*3*).

Scheme 1: Sequence of the Leadzyme Construct Used in This and Previous (*6*) Work[a]

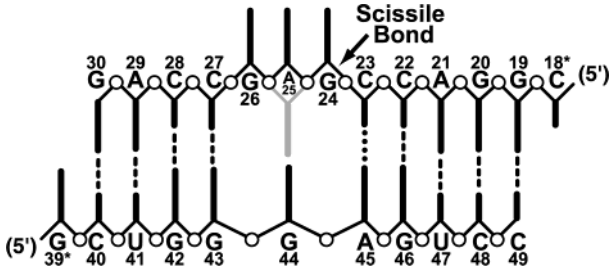

[a] Derived from LZ4 of the *in vitro* selection results (*2*). Vertical dashed lines represent Watson−Crick base pairs; the dotted line represents a non-Watson−Crick base pair between A45 and C23. The alternative flipped-in conformation of A25 observed by NMR (*8*) is shown gray.

The three-dimensional X-ray crystallographic (*6*) and solution NMR (*7*, *8*) structures of leadzyme constructs reveal essentially an RNA duplex with one non-Watson−Crick base pair (dotted line between A45 and C23, Scheme 1) and a three-nucleotide bulge (G24, A25, and G26), with the scissile phosphodiester bond at the junction between the duplex and the bulge. Additionally, the NMR data showed that in solution, the nucleotides of the bulge are relatively mobile,

† This work was supported by NIH Grant AI-30606 to D.B.M. and by a Life Sciences Research Foundation Burroughs Wellcome Fund postdoctoral fellowship and NIH Grant GM-63162 to J.E.W.

* To whom correspondence should be addressed: Department of Structural Biology, Stanford University School of Medicine, Stanford, CA 94305. Telephone: (650) 723-6589. Fax: (650) 723-8464. E-mail: Dave.McKay@Stanford.edu.

‡ Stanford University School of Medicine.

§ University of Rochester Medical Center.

10.1021/bi0300783 CCC: $25.00
Published on Web 07/25/2003

and signals indicating a conformer forming a non-Watson−Crick base pair between A25 and G44 were observed (*8*, *9*) ("flipped-in" conformation in gray, Scheme 1). The X-ray structure showed two crystallographically independent molecules in which the three-nucleotide bulges were in substantially different conformations in the asymmetric unit of hexagonal crystals of space group $P6_122$ (*6*).

The general importance of metal ions that participate in both structural and catalytic roles in ribozymes has been reviewed (*10*). In the previous leadzyme crystal structure at 2.7 Å resolution (*6*), metals used as heavy atom derivatives, as well as Mg^{2+} ions endogenous to the crystal growth and stabilization solutions, were revealed at several specific RNA binding sites, albeit at a resolution that precluded a precise description of metal−ligand interactions. When crystals were soaked briefly in solutions with divalent lead compounds, a single Pb^{2+} ion was seen bound at a site remote from the scissile bond in one conformer of the leadzyme. Extended soaks with Pb^{2+} resulted in crystal disorder due to Pb^{2+}-dependent bond cleavage at the scissile linkage. Such catalytic activity precludes the possibility of a structure determination in the presence of Pb^{2+} trapped at the active site in these crystals. However, several sites were found for Ba^{2+} ions, including a single location near the scissile phosphodiester bond, which was observed in only one of the leadzyme conformers in the asymmetric unit [denoted "molecule 2" in an earlier description (*6*)]. Simple modeling revealed that if a Pb^{2+} ion were bound at the site occupied by Ba^{2+}, relatively modest conformational rearrangements that could be accomplished by a change of the ribose sugar pucker would align the 2′-hydroxyl of the C23 ribose for in-line nucleophilic attack on the scissile G24 phosphodiester bond, thereby allowing the cleavage reaction to proceed by a pathway similar to that originally proposed for the hammerhead and hairpin ribozymes (*11*). Notably, the cleavage site of the other conformer of the leadzyme ("molecule 1") was in a substantially different conformation that would neither bind a catalytic ion nor catalyze bond cleavage readily. These two conformers, the first of which bound ions near the active site in a manner thought to mimic Pb^{2+}, were termed "precatalytic" and "ground state", respectively. We will retain this nomenclature, with the caveat that they represent only two of an ensemble of solution conformations likely to be adopted by the leadzyme.

In this study, we have extended the resolution of the leadzyme structure to 1.8 Å resolution, allowing us to delineate the RNA binding interactions and solvent coordination of metal ions precisely. We have also determined the structure of the leadyzme to 1.8 Å in the presence of Sr^{2+}, which, with an ionic radius nearly identical to that of Pb^{2+} [1.13 Å for Sr^{2+} and 1.12 Å for Pb^{2+} (*12*)], should mimic the Pb^{2+} ion binding, although not necessarily electronically or catalytically (*13*). We find that Mg^{2+} binds in the duplex major groove of the leadzyme at structural sites, as well as at a site that appears to inhibit leadzyme catalysis. Several Sr^{2+} binding sites have been located, including one near the scissile phosphodiester bond in the precatalytic conformation of the leadzyme, but not in the ground state conformation. On the basis of the results presented here, we suggest participation of metal ions as remote site, or "allo site", regulators of catalytic activity, in addition to direct participation of a single Pb^{2+} ion in the catalytic mechanism. This proposal is in lieu of the alternative two-metal ion mechanism of leadzyme catalysis that has been proposed (*4*, *5*).

EXPERIMENTAL PROCEDURES

RNA Synthesis, Purification, and Crystallization. RNA oligonucleotides were generated by chemical synthesis (Howard Hughes Medical Institute Biopolymer/Keck Foundation Biotechnology Resource Laboratory, Yale University, New Haven, CT), shipped frozen in basic solution containing ammonium hydroxide, deprotected, purified, and desalted in-house by methods that have been described previously (*14*). Following purification and desalting, individual strands of RNA were dissolved in 10 mM sodium cacodylate buffer (pH 6.0) to a final working concentration of 1 mM, based on calculated extinction coefficients of 115 and 139 mM^{-1} cm^{-1} at a λ of 260 nm for the 11-mer and 13-mer (Scheme 1), respectively. The RNA was stored in solution at −20 °C.

For crystallization, all stock reagent solutions were filtered (pore size of 0.2 μm) and autoclaved except $Mg(OAc)_2$, which was filtered only. Crystals were grown by hanging drop vapor diffusion at 20 °C using a precipitant solution consisting of 21−24% (v/v) MPD,[1] 20 mM $Mg(OAc)_2$, 1 mM spermine-HCl, and 50 mM sodium cacodylate derived from a 1.0 M pH 6.0 stock solution, as described previously (*6*). The following refinements to the crystal growth protocol yielded crystals larger than those described previously: the initial RNA duplex concentration was decreased from 0.8 to 0.4 mM prior to the addition of precipitant, and the initial crystallization hanging drop size was increased from 1−2 to 5−6 μL, resulting in sparser nucleation, followed by growth of hexagonal rods with dimensions of 0.05 mm × 0.05 mm × 0.75 mm after approximately 1 month. Such crystals diffract anisotropically to approximately 1.6 Å resolution along the c^* axis and 1.8 Å resolution along the a^* axis using a high-flux synchrotron beamline.

X-ray Crystallographic Data Collection and Processing. Crystals were adapted in a single transfer step to a synthetic mother liquor containing 35% (v/v) MPD, 100 mM Na-MES (pH 6.0), and divalent ions [either 20 mM $Mg(OAc)_2$ ("Mg-only") or 20 mM $Mg(OAc)_2$ and 20 mM $SrCl_2$ ("Mg+Sr")]. The crystals adapted to Mg+Sr were first transferred to a Mg-only solution for approximately 30 min, and subsequently into an Mg+Sr solution for an additional 30 min. Respective metal-soaked samples were flash-frozen in a stream of dry N_2 gas at −173 °C. Crystallographic data were collected using a Mar 345 image-plate detector on beamline 9-1 of the Stanford Synchrotron Radiation Laboratory (SSRL). Both the Mg-only and the Mg+Sr data sets were collected from single crystals in two passes. The first pass was designed to record high-resolution reflections and utilized an exposure time of 5 min/deg with a crystal-to-detector distance of 240 mm. The second pass was designed to record low-resolution diffraction data that were overloaded on the first pass and utilized an exposure time of 30 s/deg with a crystal-to-detector distance of 340 mm. Integrated intensities were derived from the raw frame data and scaled

[1] Abbreviations: MPD, 2-methyl-2,4-pentanediol; MES, 2-(*N*-morpholino)ethanesulfonic acid; MOPS, 3-(*N*-morpholino)propanesulfonic acid; OAc, acetate ion; PDB, Protein Data Bank; rmsd, root-mean-square deviation; SSRL, Stanford Synchrotron Radiation Laboratory.

Table 1: X-ray Data and Refinement Statistics (Space Group $P6_1$)

	20 mM Mg^{2+} X-ray data set ($\lambda = 0.98$ Å)	20 mM Mg^{2+} + 20 mM Sr^{2+} X-ray data set ($\lambda = 0.98$ Å)
unit cell (Å)	$a = b = 60.1$, $c = 133.1$	$a = b = 60.1$, $c = 132.9$
no. of observations	286623	228937
no. of independent reflections	25179 (34.0−1.8 Å)	24885 (33.9−1.8 Å)
(average *I*)/(average error in *I*)		
lowest to 1.80 Å[a]	63686.1/2991.5 = 21.3	281047.2/12688.1 = 22.5
1.83−1.80 Å	2760.9/595.0 = 4.6	16031.2/3492.7 = 4.6
R_{sym}[b] (%) (37.0−1.80 Å)	4.0	3.5
R_{sym} (%) (1.83−1.80 Å)	27.2	16.4
Refinement Statistics (lowest to 1.80 Å, $F \geq 0$)		
overall completeness (%)	95.2	94.1
completeness (%) (1.86−1.80 Å)	87.4	76.5
no. of RNA atoms (solvent)	2072 (416)	2072 (407)
no. of Mg(II) atoms	10	10
no. of Sr(II) atoms	−	6
overall R_{factor}[c]/R_{free}[d] (1.86−1.80 Å)	20.3/22.4 (28.5/32.7)	21.0/22.0 (26.8/27.1)
rmsd from ideal geometry		
bond lengths (Å)	0.007	0.005
angles (deg)	1.20	1.20
impropers (deg)	1.77	1.72
average *B*-factor (Å^2)		
RNA atoms	27.9	26.1
solvent atoms	41.5	39.4
Mg(II) atoms	39.9	37.7
Sr(II) atoms	−	68.4
anisotropic *B*-factor tensor	$B_{11} = B_{22} = 4.4$; $B_{33} = -8.9$	$B_{11} = B_{22} = 4.5$; $B_{33} = -9.0$
coordinate error (Å)		
cross-validated Luzzati plot	0.37	0.36
cross-validated SIGMAA	0.38	0.36

[a] Numbers in parentheses refer to the resolution range of the data. The lowest resolution for experimental data was 34.0 Å for Mg-only and 33.9 Å for Mg+Sr; the lowest-resolution data used in refinement were at 34.0 Å for Mg-only and 28.1 Å for Mg+Sr. [b] $R_{sym} = 100 \times \sum_{hkl}|I_j - \langle I_j \rangle|/\sum|I_j|$. [c] $R_{factor} = 100 \times \sum|F_o - F_c|/\sum|F_o|$, where F_o and F_c are the observed and calculated structure factor amplitudes, respectively. [d] R_{free} is the R_{factor} calculated from 8.0% of the data, selected randomly and excluded from the structure refinement.

with the programs DENZO and SCALEPACK (*15*); data collection statistics are summarized in Table 1.

Structure Determination and Refinement. Crystallographic calculations were performed with the programs CNS (*16*) and CCP4 (*17*). Model building was conducted using the molecular graphics program O (*18*, *19*). The Mg+Sr leadzyme crystal structure was determined using coordinates from the previously reported leadzyme crystal structure refined to 2.7 Å resolution in space group $P6_122$ (PDB entry 429D) (*6*). A temperature factor of 24 Å^2 was initially assigned to all atoms based on a Wilson plot computed within CCP4, and 8% of the reflections were assigned randomly to a test set for R_{free} calculations. First, rigid body refinement was carried out by treating each of the four RNA strands as separate objects. Amplitude-based maximum likelihood target minimization was conducted as implemented in CNS using data between 3.5 and 28.1 Å resolution. Subsequently, the model was subjected to Cartesian simulated annealing using CNS at an initial temperature of 2500 °C, and then Powell minimized using all data to 1.8 Å resolution. Model adjustments were performed manually in O using SIGMAA-weighted $2F_o - F_c$ and $F_o - F_c$ electron density maps.

At 1.8 Å resolution, omit maps revealed that the nucleotide base of G26 of one leadzyme molecule (molecule 1, chains A and B of PDB entry 429D), which appeared to be partially disordered at 2.7 Å resolution (*6*), is well-defined and adopts both *syn* and *anti* alternate conformations (Figure 1a). Specifically, G26 bases from two adjacent molecules are coplanar and can form a pair of hydrogen bonds with one nucleotide base in the *anti* conformation and the other in the *syn* conformation, but a steric clash precludes both nucleotides from simultaneously adopting the *anti* conformation (Figure 1b). This interaction is between two molecules that are related by a crystallographic 2-fold axis of rotation in space group $P6_122$. However, the *syn*/*anti* alternative conformations adopted by the G26 base pair result in a subtle but significant breakdown in space group symmetry, from the original $P6_122$ with two independent molecules per asymmetric unit. Therefore, the structure was re-refined from the original PDB entry 429D in space group $P6_1$ with four molecules per asymmetric unit. The diffraction data and test data test were expanded appropriately. The four independent molecules in the asymmetric unit were denoted Mol0−Mol3 (Figure 1c). Atomic occupancies for the two G26 *syn*/*anti* conformer pairs of Mol0 and Mol3 were set to 0.5. [Strictly speaking, we find equal populations of the *syn* and *anti* conformers of G26 for both Mol0 and Mol3 will, on average, retain the crystallographic 2-fold axis and the $P6_122$ space group. However, the 2-fold axis (Figure 1c) would generate an *anti*/*anti* pair with an occupancy of 0.5 in the refinement, which would result in substantial steric clash. Therefore, refinement was completed in the $P6_1$ space group to provide a more comprehensive molecular model that does not constrain atoms on the dyad special position.]

Water molecules were added by use of CNS using the criteria that solvent peak heights were $\geq 2.75\sigma$ in $F_o - F_c$ electron density maps and interatomic distances between solvent and O or N were greater than 2.55 Å but less than 3.75 Å. All waters were inspected in $F_o - F_c$ and $2F_o - F_c$ maps and adjusted manually to meet a requirement of one

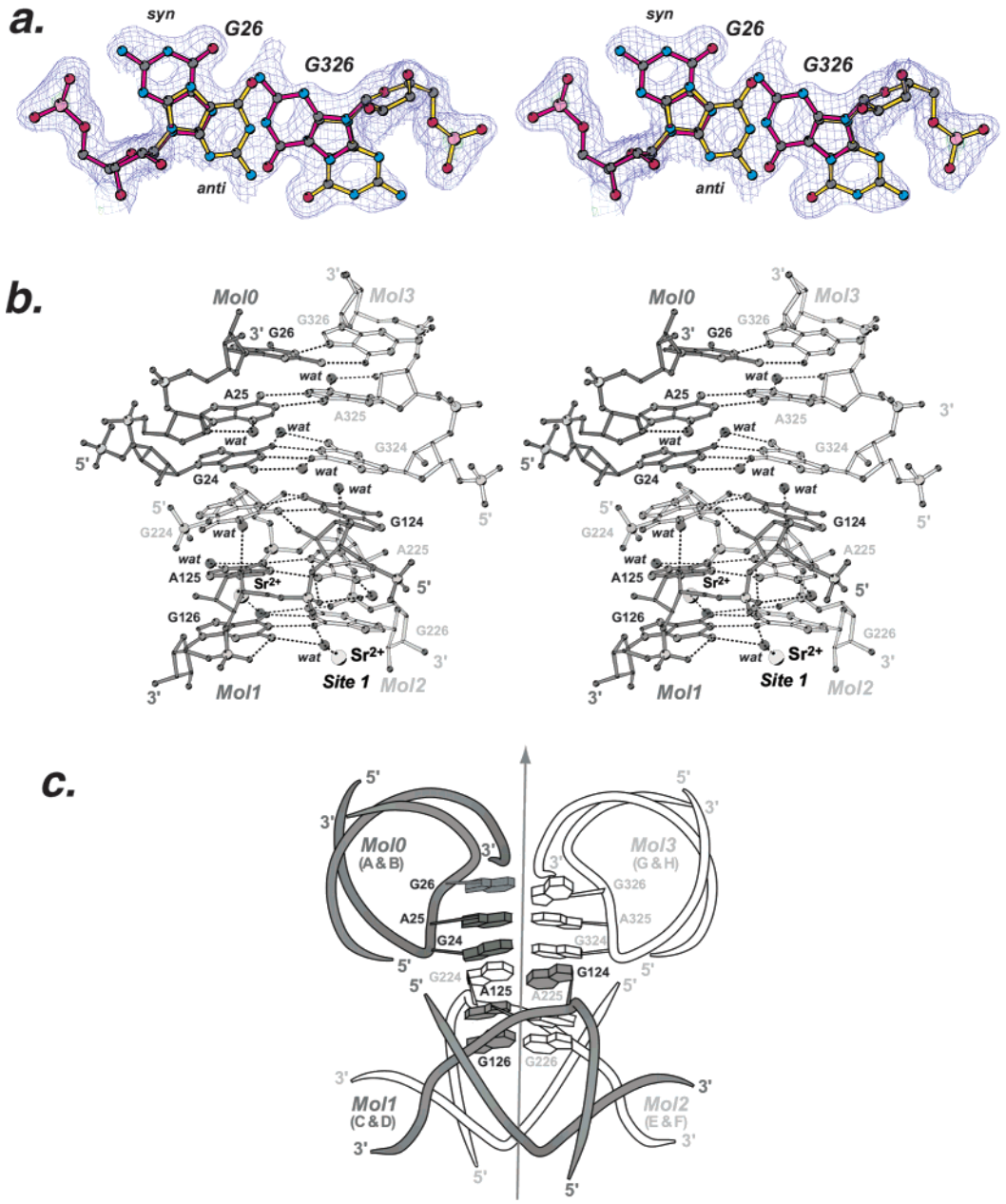

FIGURE 1: Alternate conformations for G26 at the molecular interface. (a) SIGMAA-weighted $2F_o - F_c$ electron density contoured at 1.0σ showing the alternate conformations of G26 observed in Mol0 and Mol3 in the Mg-only structure. In the molecular model, the bases for one conformation (G26 *syn* and G326 *anti*) are colored red and for the alternate conformation yellow. (b) Stereographic ball-and-stick picture of the intermolecular interactions of the bases of the trinucleotide bulges. Only one of the two alternate conformations is shown for G26 and G326. Coordinates from the Mg+Sr structure were used to make the structure. (c) Schematic diagram of the intermolecular packing of the trinucleotide bulges around the pseudo-2-fold axis for the four leadzyme protomers in the asymmetric unit of space group $P6_1$. Chain designations A−H are labeled according to PDB naming conventions in 1NUJ and 1NUV. This figure was made with the program BOBSCRIPT (*29*).

or more hydrogen bonds with reasonable geometry. The model was adjusted manually with alternating cycles of minimization and individual temperature factor refinement. The Mg-only structure was refined in a manner similar to that of the Mg+Sr structure, beginning with space group $P6_1$.

At 1.8 Å resolution, Mg^{2+} ions were identified in both structures by characteristic octahedral coordination geometry (Figure 2a) and oxo−metal distances consistent with those observed in other RNA structures (*10*). Sr^{2+} ions were identified in the Mg+Sr structure in difference Fourier maps computed from F_{obs}^{Mg+Sr} and $\alpha_{calc}^{Mg-only}$. Residual peaks in these maps indicated 14σ electron density with geometry and metal−ligand distances inconsistent with Mg^{2+}, but comparable to values reported for crystallographic structures of complexes of Sr^{2+} with small molecules (*12*). All ions and ligands were verified in $F_o - F_c$ simulated annealing omit maps using the refined model phases (Figure 2). Final refinement statistics are provided in Table 1. Coordinates and structure factor amplitudes have been deposited in the Protein Data Bank (entries 1NUJ and 1NUV) for the Mg-only and Mg+Sr structures, respectively.

Activity Assays. The leadzyme cleavage activity was assayed at 37 °C with 10 μM duplex RNA in a reaction buffer consisting of 10 mM $Mg(OAc)_2$ and 15 mM MOPS-K (pH 7.0). Lyophilized RNA powder was suspended in MilliQ

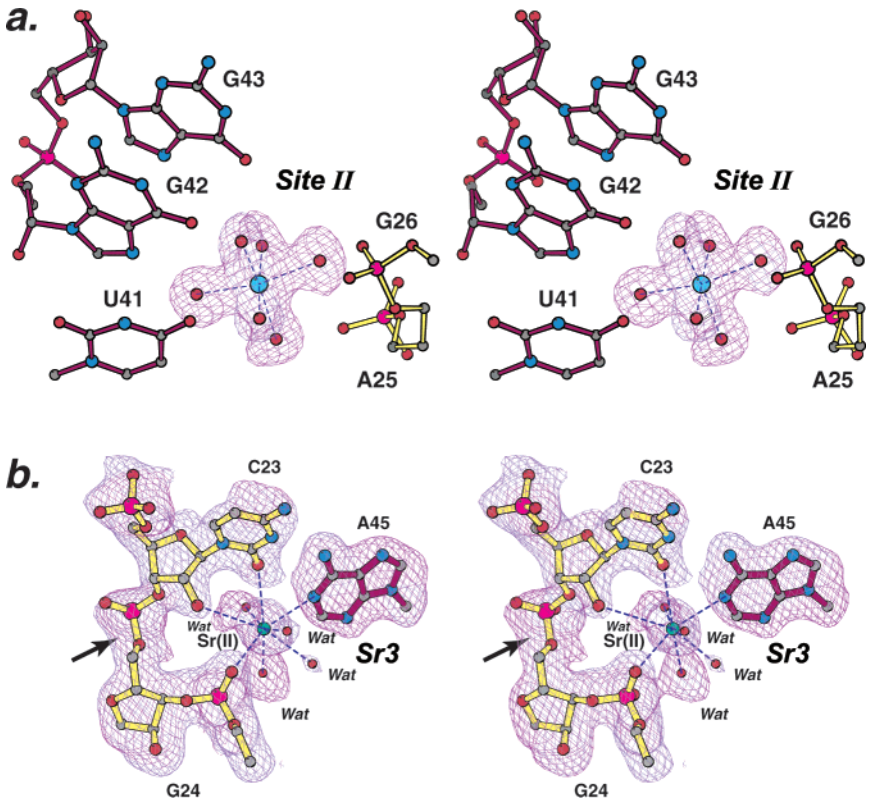

FIGURE 2: Stereodiagrams of representative $F_o - F_c$ simulated annealing omit maps in which the respective Sr^{2+} and Mg^{2+} metal ions, as well as surrounding ligands, were removed. Electron density maps were calculated with SIGMAA coefficients. RNA is depicted with ball-and-stick models; nucleotides from the ribozyme strand are colored maroon and from the substrate strand yellow. Dashed lines represent inner sphere ligand contacts to the metals. (a) Representative $Mg(H_2O)_6^{2+}$ binding site near the bulged loop contoured at 2.0σ. A cyan sphere represents Mg^{2+}. (b) Sr^{2+} binding site near the scissile bond contoured at 2.5σ. An arrow shows the site of cleavage. A cyan sphere represents Sr^{2+}. This figure was made with the program BOBSCRIPT (*29*).

water, diluted with reaction buffer to a final volume of 500 μL, and incubated at 37 °C for at least 30 min. The reaction was then initiated by adding $Pb(OAc)_2$ and/or $SrCl_2$ to give a final concentration of 0.20 mM Pb^{2+}, 0.20 mM Sr^{2+}, or 0.10 mM Pb^{2+} and 0.10 mM Sr^{2+}. Aliquots were collected at 3, 20, 60, and 120 min; the reaction was quenched by freezing in liquid nitrogen, and the mixture was lyophilized to dryness. RNA strands were resolved by electrophoresis on 20% polyacrylamide gels and visualized by silver staining (*14*).

RESULTS

X-ray Diffraction. The improved diffraction of leadzyme crystals to ~1.6 Å resolution along the *c** axis and 1.8 Å resolution along the *a** axis has allowed refinement of precise, high-resolution structures, both in the presence of magnesium as the sole divalent cation in the crystals and in the presence of magnesium and strontium. The larger crystal volume, in comparison to crystals used in earlier work (*6*), and possibly also the slower kinetics of crystal growth, which may have improved the internal order of the crystals, contributed to the feasibility of high-resolution data collection. The crystals showed no evidence of significant radiation decay during data collection, based upon a comparison of scale factors for successive diffraction images when scaled in SCALEPACK (*15*), as well as the consistency of high-resolution X-ray diffraction resolution reported as I/σ per batch (data not shown).

The ability to distinguish alternate *syn* and *anti* conformations of the base of G26 in one pair of leadzyme molecules at 1.8 Å resolution (Figure 1a) necessitated refinement in space group $P6_1$ with four molecules per asymmetric unit (Figure 1c), as described in Experimental Procedures. Crystals grown under identical conditions were used for both the Mg-only and Mg+Sr structures, and the symmetry breakdown was similar in both cases. The resulting crystal structures of the Mg-only and Mg+Sr forms of the leadzyme are nearly identical, with the exception of Sr^{2+} binding; the respective structures superimpose with an average root-mean-square deviation of 0.306 Å for all RNA atoms in the asymmetric unit (computed with LSQKAB in CCP4). Therefore, the Mg-only structure provides a control experiment for assessing the locations of, and conformational changes induced by, Sr^{2+} ions.

Overall, no substantial structural differences are observed between Mol0 and Mol3, which were termed molecule 1 and its symmetry-related counterpart in space group $P6_122$, respectively (*6*), nor do we see major differences between Mol1 and Mol2, previously termed molecule 2 and its symmetry-related mate, respectively. To simplify the discussion that follows, we describe only the two different conformations of the leadzyme (Mol0/Mol3, the "ground state"; Mol1/Mol2, the "precatalytic" state) rather than all four protomers of the asymmetric unit.

Magnesium Binding Sites. Three fully hydrated Mg^{2+} ions were identified in the leadzyme molecule in the ground state conformation (labeled I−III, Figure 3a). Mg^{2+} ions are also

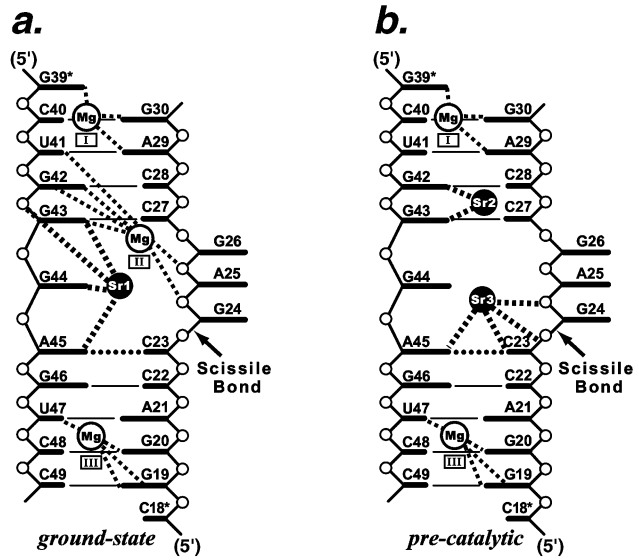

FIGURE 3: Schematic drawing of the interactions between metal ions and the leadzyme RNA. The Mg^{2+} sites are labeled in Roman numerals (I−III) and were the same in the Mg-only and Mg+Sr structures; the Sr^{2+} sites, present in only the Mg+Sr structure, are labeled with Arabic numerals (1−3). Nucleotide bases are depicted as bold lines (short for pyrimidine and long for purine). Thin lines between bases represent Watson−Crick hydrogen bonds, whereas a dotted line represents a non-Watson−Crick interaction between C23 and A45. Empty spheres and intervening lines represent the phosphate−ribose backbone. Thick dashed (black) lines represent hydrogen bonds between nucleotide bases and waters within the inner hydration sphere of $Mg(H_2O)_6^{2+}$. Thick dashed (gray) lines represent direct ionic interactions between nucleotides and Sr^{2+}: (a) ground state structure and (b) precatalytic structure.

found at sites I and III of molecules in the precatalytic conformation (Figure 3b). Each of the Mg^{2+} ions binds in the major groove of the RNA duplex via contacts mediated by the octahedral hydration sphere. In all instances, either three or four of six waters in the primary hydration sphere of magnesium form four hydrogen bonds directly to the major groove face of the RNA bases (Figures 3 and 4, sites I−III). At each site, three RNA bases participate with hydrogen bonds, whereas only at one site (site II) do nonbridging phosphate oxygens participate. The remainder of the H_2O−Mg^{2+} ligands form hydrogen bonds to second-sphere waters that mediate contacts to either nucleotide bases or phosphate oxygens.

A shared feature of Mg^{2+} ions bound to sites I and III is the manner in which they interact with tandem purines (A29 and G30 for site I and G19 and G20 for site III). A pair of adjacent H_2O molecules in the first coordination shell of the metal ion hydrogen bonds to both N7 and either O6 (of G19) or N6 (of A29) of the first (5′-proximal) nucleotide of the tandem purines. This bidentate interaction is facilitated by the approximate congruence of the 3.1 Å spacing between N7 and the exocyclic O6 (of guanosine) or N6 (of adenosine) of the base, and the 2.8−3.0 Å spacing between adjacent octahedrally bound H_2O molecule in the first hydration shell of the Mg^{2+} ion. A third H_2O molecule in the first hydration shell hydrogen bonds to O6 of guanosine of the 3′-proximal nucleotide of the tandem pair, and also to a well-defined H_2O molecule which, in turn, hydrogen bonds to N7 of the guanosine. Thus, through three H_2O molecules of the inner coordination shell of the Mg^{2+} ion, and one bridging H_2O molecule, the Mg^{2+} ions at sites I and III interface with all the available hydrogen bonding groups presented in the major groove by the bases of the tandem purine pair.

These interactions on one side of the major groove position a fourth H_2O molecule of the first hydration shell for specific interactions on the other side of the groove. Specifically, an H_2O molecule hydrogen bonds to an exocyclic group of the base that is complementary to the nucleotide following (i.e., 3′ to) the tandem purines (Figure 3). At site III, this is O4 of U47; at site I, it is O6 of G39 (which forms a Watson−Crick base pair with C18 of a neighboring molecule that, through intermolecular crystal packing, extends the RNA duplex stem beyond the termini of the oligonucleotide strands).

The Mg^{2+} ion at site II, present in only the ground state conformation of the leadzyme, also binds a pair of tandem purines, G42 and G43, with two adjacent inner sphere H_2O molecules hydrogen bonding to N7 and O6 of G42 in interactions similar to those seen at sites I and III. However, other interactions are distorted with respect to those seen at sites I and III. O6 of G43 does not hydrogen bond with a separate H_2O molecule, but rather shares an H_2O molecule with O6 of G42, while O4 of U41, the base preceding the tandem purines, hydrogen bonds one of the inner sphere H_2O molecules. Two other inner sphere H_2O molecules hydrogen bond to nonbonded phosphate oxygens of A25 and G26 of the three-nucleotide bulge of the complementary oligonucleotide strand.

Strontium Binding Sites. When Sr^{2+} is included along with Mg^{2+} in the crystal stabilization solution, Sr^{2+} ions bind several sites on the leadzyme without displacing or significantly perturbing the Mg^{2+} ions that are seen in the absence of Sr^{2+} (Figures 3 and 5). A single Sr^{2+} ion, labeled Sr1, binds to the leadzyme in the ground state conformation, adjacent to Mg^{2+} ion binding site II. H_2O molecules in the first hydration sphere of the metal ion hydrogen bond to N7 of G43, N7 and O6 of G44, and N6 of A45, as well as a nonbridging phosphate oxygen of G43 (Figure 5a,d).

Two Sr^{2+} ions bind to the leadzyme in the precatalytic conformation. One, labeled Sr2, binds the tandem guanosines G42 and G43 that are occupied by the Mg^{2+} ion at site II in the ground state (Figure 3). Specifically, three H_2O molecules in the first coordination shell of the Sr^{2+} ion hydrogen bond to N7 of G42, the exocyclic O6 of G42, and N7 of G43 (Figure 5b,e). The interaction of the hydrated Sr^{2+} ion with tandem purines is reminiscent of, but not identical to, the interactions between Mg^{2+} ions and tandem purines described above.

An additional Sr^{2+} ion (Sr3) binds near the scissile bond; it lies between, and ligates directly to, N1 of A45 and the *pro*-S_p nonbridging phosphate oxygen of A25, with metal−ligand distances of ∼2.5 Å. In addition, three H_2O molecules are visible in the first coordination shell, and this Sr^{2+} ion is 3.8 Å from the oxygen of the 2′-hydroxyl of the ribose of C23, from which a proton must be abstracted in the first step of the leadzyme bond cleavage reaction (Figure 5c,f). The binding of Sr3 coincides with modest but significant alterations in the conformation of the phosphodiester backbone in the vicinity of the scissile bond; most notably, the sugar pucker of the C23 ribose switches from C2′-*endo* in the Mg-only structure to C3′-*endo* in the Mg+Sr structure. In contrast, minimal structural change is observed throughout the remainder of the molecule. The subtle structural changes

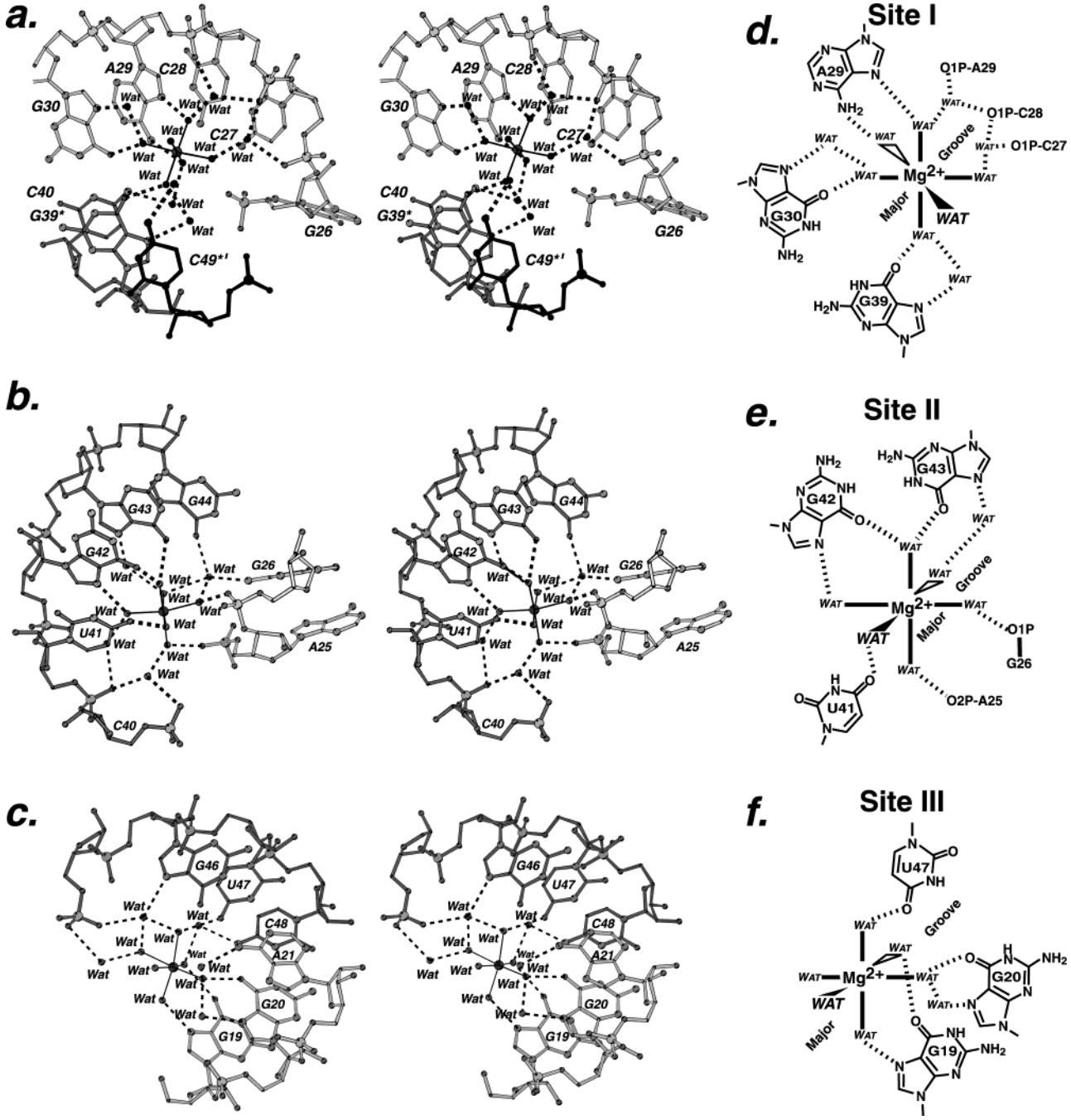

FIGURE 4: Stereodiagrams and schematic drawings of the three Mg^{2+} binding locations denoted I−III. In all diagrams, dashed lines represent putative hydrogen bonds. Solid lines between Mg^{2+} and water (black spheres or labeled *Wat*) indicate solvent in the first hydration sphere. In the stereodiagrams, RNA is depicted as ball-and-stick models. Direct inner sphere ligand contacts between RNA and the hydrated Mg^{2+} are depicted schematically to the right of each stereo drawing: (a) stereoview of site I, (b) stereoview of site II, (c) stereoview of site III, and (d−f) schematic figures to accompany magnesium sites I−III, respectively. This figure was made with the program BOBSCRIPT (*29*).

that we see when strontium occupies the preformed catalytic ion binding site attest to the capacity of metal ion binding to alter the local conformation of the cleavage site.

Effect of Strontium on Leadzyme Activity. Leadzyme cleavage activity was assayed as described in Experimental Procedures. In the presence of 0.2 mM Pb^{2+}, the substrate strand of the leadzyme duplex is cleaved completely within 20 min, while in the presence of Sr^{2+}, no significant cleavage is observed after 2 h (data not shown). Assays in the presence of equimolar Pb^{2+} and Sr^{2+} showed cleavage, but with a significant reduction in rate compared to the rate with Pb^{2+} alone. Although the limited quantities of RNA that were available precluded further steady state characterization of the effects of Sr^{2+} on the leadyzme activity, a detailed study to determine whether Sr^{2+} acts as a classical competitive inhibitor of the Pb^{2+}-dependent catalytic activity would be of interest in the context of the structural results reported here.

DISCUSSION

Binding of $Mg(H_2O)_6^{2+}$ and Other Ions to Tandem Purines. Early work revealed the binding of cobalt hexammine [$Co(NH_3)_6^{3+}$, a structural mimic of $Mg(H_2O)_6^{2+}$] to tandem purine bases in the major groove of yeast phenylalanine tRNA at 3.0 Å resolution (*20*). The tRNA structure has recently been extended to higher resolution, defining the

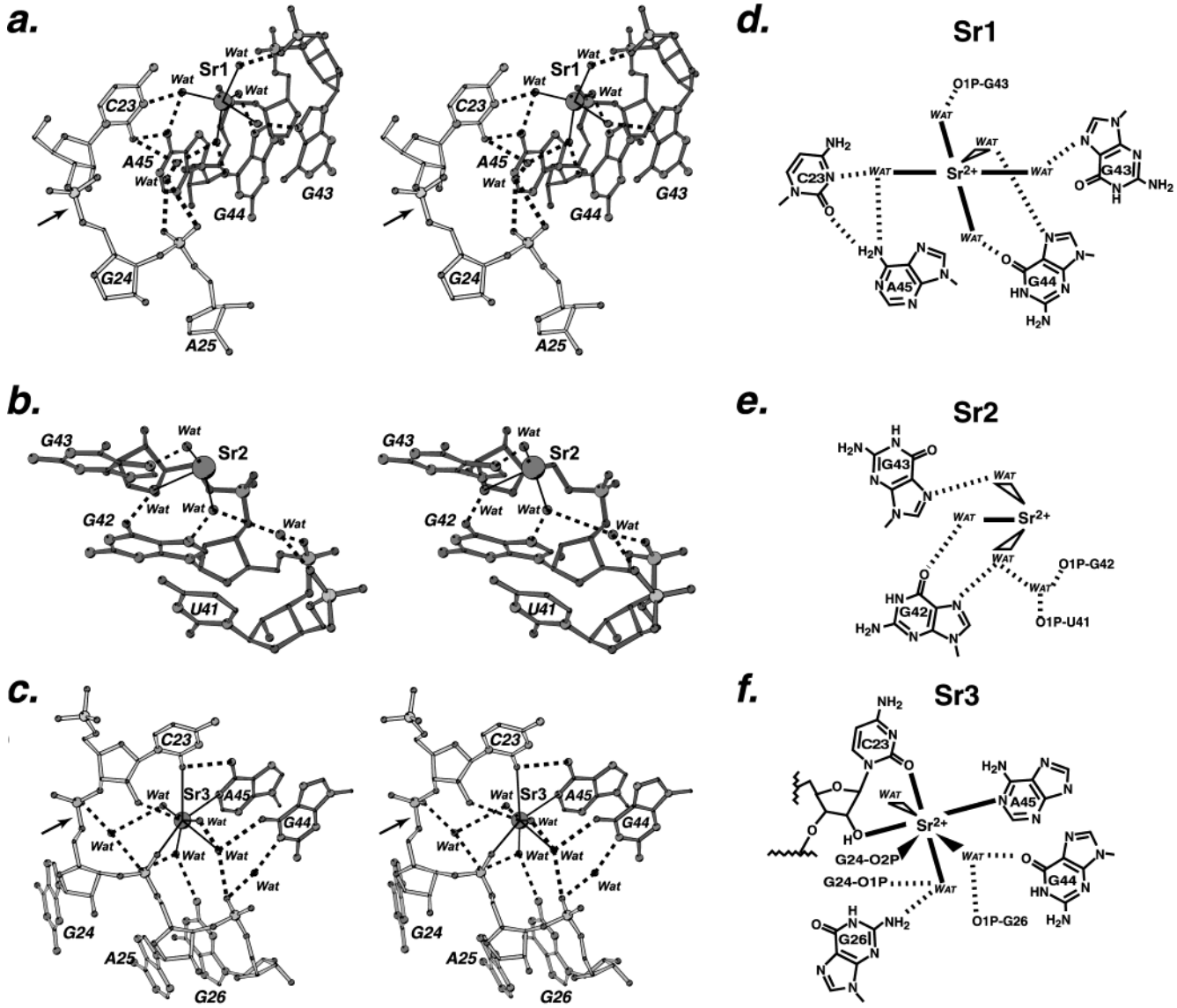

FIGURE 5: Stereodiagrams and schematic drawings of the three Sr^{2+} binding sites. The three Sr^{2+} binding locations are denoted Sr1−Sr3. In all diagrams, dashed lines represent putative hydrogen bonds. Solid lines between Sr^{2+} and water (black spheres or labeled *Wat*) indicate solvent in the first hydration sphere. In the stereodiagrams, RNA is depicted as ball-and-stick models. Direct inner sphere ligand contacts between RNA and the hydrated Sr^{2+} are depicted schematically to the right of each stereodrawing: (a) stereoview of site 1, (b) stereoview of site 2, (c) stereoview of site 3, and (d−f) schematic figures to accompany strontium sites 1−3, respectively. This figure was made with the program BOBSCRIPT (*29*).

solvent and metal ion interactions more precisely (*21*, *22*); a magnesium ion is seen to bind tandem purines G3 and G4 and to form a bridge to U68 of the complementary RNA strand in a manner similar to what we see in the leadzyme.

Other work has shown binding of osmium hexammine, $Os(NH_3)_6^{3+}$, to tandem guanosines in the P4−P6 domain of a group I intron at 2.8 Å resolution (*23*). Although the resolution of the diffraction data precluded direct observation of the coordination geometry in these cases, model building which optimized hydrogen bonding between the hexammines and the RNA supports a mode of binding in which a *cis* pair of amine ligands contribute hydrogen bond donors to the N7 and O6 hydrogen bond acceptors of adjacent purine bases.

Within the B domain of the hairpin ribozyme, two binding sites for $Mn(H_2O)_6^{2+}$ have been delineated by NMR; at one of these sites, the hydrated manganese ion is modeled to bind tandem guanosines with inner sphere H_2O molecules hydrogen bonding to N7 and O6 of the guanine bases, in a manner similar to osmium hexammine binding to a site in the group I intron domain (*24*). The general scheme whereby mimics of $Mg(H_2O)_6^{2+}$ bind tandem purines through interactions with the major groove hydrogen bond acceptors of the bases is consistent with the data we present here. However, at 1.8 Å resolution, we are able to observe the coordination geometry and metal−ligand interactions directly. These data reveal, among other details, the manner in which hydrated metal ions can "bridge" the major groove and thereby ligate complementary strands of RNA when they bind tandem purines on one strand.

Model for Allo Site Modulation of Leadzyme Activity. The manner in which metal ions bind the leadzyme structure suggests a mechanism whereby they may act as modulators of catalytic activity. A Mg^{2+} ion binding at site II forms a bridge from the bases of G42 and G43 in the ribozyme strand to the phosphodiester backbone of the trinucleotide bulge in the substrate strand, constraining it to an apparent noncatalytic conformation. Displacement of magnesium from the

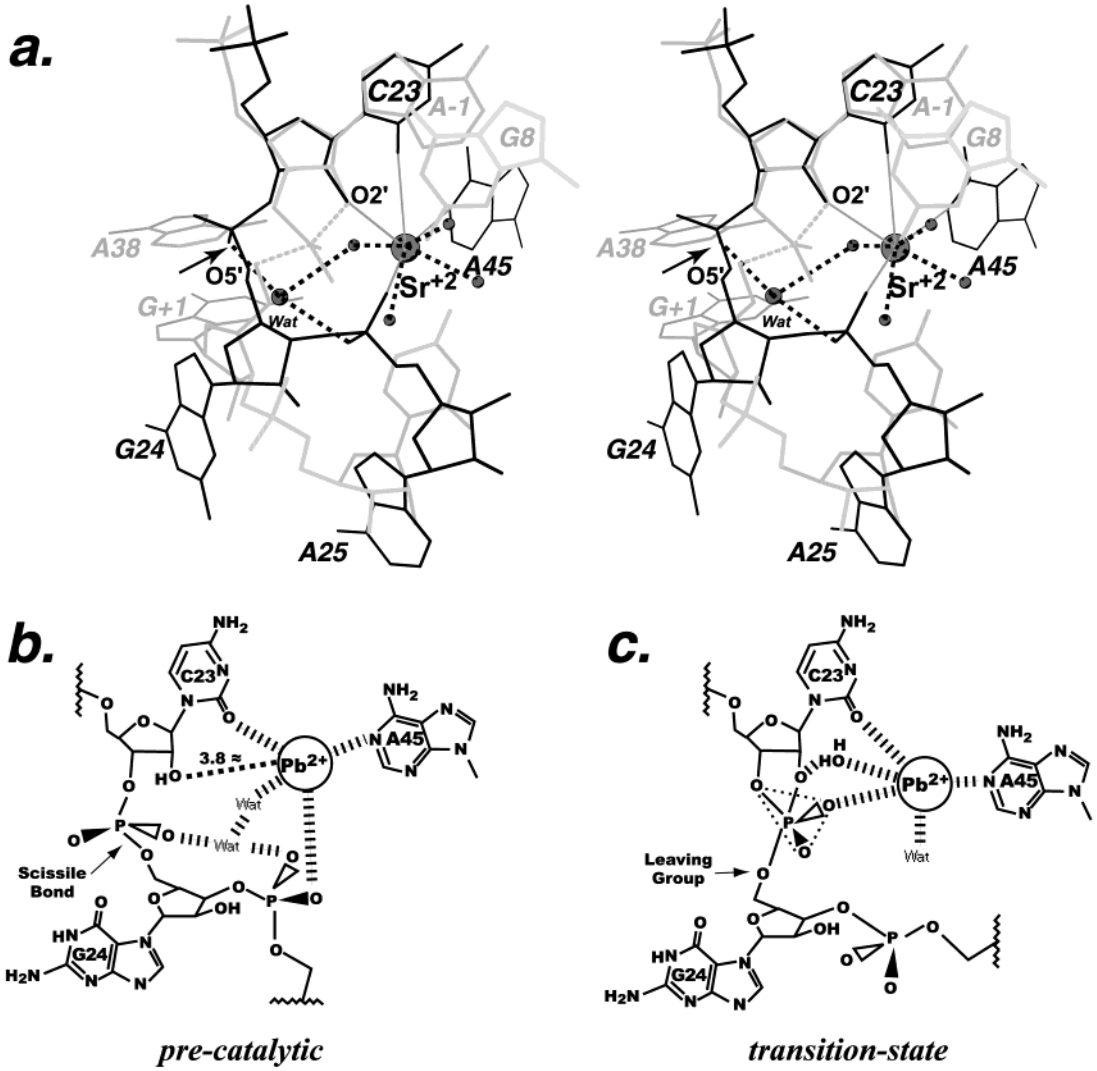

FIGURE 6: Model for lead-dependent ribozyme catalysis. (a) Stereoview of a superposition of the precatalytic leadzyme structure with that of the hairpin ribozyme in complex with vanadate, a mimic for the transition state geometry of the reaction. The leadzyme is depicted in black bonds; the hairpin ribozyme (PDB entry 1M5O) is shown in gray. (b) Proposed precatalytic conformation in which Pb^{2+} interacts directly with the 2′-hydroxyl group of C23. (c) Proposed transition state arrangement. This figure was made with the program BOBSCRIPT (*29*).

Scheme 2: Proposed Scheme for Modulation of Leadzyme Activity by Metal Ions

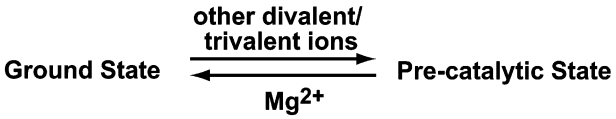

tandem purines G42 and G43 by a competing ion that does not form a bridge to the substrate strand through similar interactions with the phosphodiester backbone could untether the trinucleotide bulge and allow it to relax into a precatalytic conformation. In the Mg+Sr structure reported here, we observe that an Sr^{2+} ion binds G42 and G43 in the precatalytic conformation of the leadzyme; in earlier work, a Pb^{2+} ion was observed at lower resolution at this site (*6*). Thus, the following scheme is suggested, wherein Mg^{2+} ions will shift the equilibrium toward ground state conformations, and metal ions that can displace Mg^{2+} from site II without constraining the backbone of the trinucleotide bulge themselves will shift the equilibrium toward precatalytic conformations (Scheme 2).

This scheme reconciles the observation that at least two metal ions are required for the maximal catalytic rate (*4*) with the suggestion that a single catalytic ion participates directly in the chemical mechanism of bond cleavage; we propose that a second ion remote from the cleavage site enhances the reaction rate through allo site activation. It is notable that this model of modulation of activity by metal ions requires conservation of specific interactions in the duplex segment of the RNA; the emergence of conserved sequences in duplex RNA segments having generic Watson−Crick base pairs during *in vitro* selection experiments is generally overlooked until subsequent experiments reveal their functional significance.

Implications of the Structures for the Catalytic Mechanism. Although the stereochemistry of the leadzyme cleavage reaction has not been determined experimentally, the products of the first step of the reaction, a 2′,3′-cyclic phosphate and 5′-hydroxyl, are identical to the products of the hammerhead and hairpin ribozyme reactions. For the hammerhead and hairpin ribozymes, it is established that the cleavage reaction proceeds with inversion of configuration of the phosphate,

which is consistent with a reaction initiated by in-line nucleophilic attack of a ribose 2′-hydroxyl on the scissile phosphodiester bond (*11*, *25*, *26*). It is likely that the leadzyme reaction proceeds through a transition state that is similar to that of the hammerhead and hairpin. In this context, it is instructive to compare the active site geometry of the leadzyme with that of the hairpin ribozyme, structures of which have been determined that mimic both a catalytic precleavage conformation [in which bond cleavage is inhibited by a 2′−O-methyl ribose (*27*)] and a transition state conformation [with pentacoordinate vanadate substituting for the phosphate of the scissile bond (*28*)]. Superposition of the precatalytic Mg+Sr leadzyme structure with the transition state mimic of the hairpin is shown in Figure 6a.

It is apparent that the precatalytic leadzyme has a ribose conformation that is similar to that of the hairpin ribozyme and could access a similar transition state geometry through rotation of the phosphodiester backbone. This could be accomplished through a conformational change in which the active site metal ion releases the phosphate oxygen of A25 and ligates the *pro-*R_p phosphate oxygen of G24 (Figure 6b,c). Notably, this would drive the trinucleotide bulge toward a conformation that would allow base pairing between A25 and G44 of the complementary strand, consistent with the NMR observation that such a base pair forms in solution. In such a scenario, a catalytic Pb^{2+} ion binding to a precatalytic conformation of the leadzyme would exploit the flexibility of the trinucleotide bulge to pull the active site into a catalytic conformation.

The following aspects of a catalytic scenario are established by the crystal structures presented here. (a) The precatalytic conformation of the leadzyme has a preformed metal ion binding site at the active site while the ground state conformation does not, and (b) binding of Sr^{2+} at the catalytic site induces localized structural changes around the cleavage site while leaving the remainder of the structure unperturbed. We do not observe, and we presume the leadzyme cannot access without disruption of the crystal lattice, the relatively large structural rearrangement of the phosphodiester backbone that would be required to reach a transition state geometry similar to that of the hairpin ribozyme. However, the metal binding and structural rearrangements that we do observe are compatible with a catalytic mechanism of in-line nucleophilic attack by the C23 ribose 2′-hydroxyl, facilitated by a single Pb^{2+} ion. By implication, although the specific details of the dependence of the reaction on metal ions differ from those of other small ribozymes, the reaction pathway is likely to be similar.

ACKNOWLEDGMENT

Portions of this research were carried out at the Stanford Synchrotron Radiation Laboratory (SSRL), a national user facility operated by Stanford University on behalf of the U.S. Department of Energy, Office of Basic Energy Sciences. The SSRL Structural Molecular Biology Program is supported by the Department of Energy, Office of Biological and Environmental Research, and by the National Institutes of Health, National Center for Research Resources, Biomedical Technology Program, and the National Institute of General Medical Sciences. We thank the staff of SSRL for assistance.

REFERENCES

1. Pan, T., and Uhlenbeck, O. C. (1992) *Biochemistry 31*, 3887−3895.
2. Pan, T., and Uhlenbeck, O. C. (1992) *Nature 358*, 560−563.
3. Pan, T., Dichtl, B., and Uhlenbeck, O. C. (1994) *Biochemistry 33*, 9561−9565.
4. Sugimoto, N., and Ohmichi, T. (1996) *FEBS Lett. 393*, 97−100.
5. Ohmichi, T., and Sugimoto, N. (1997) *Biochemistry 36*, 3514−3521.
6. Wedekind, J. E., and McKay, D. B. (1999) *Nat. Struct. Biol. 6*, 261−268.
7. Legault, P., Hoogstraten, C. G., Metlitzky, E., and Pardi, A. (1998) *J. Mol. Biol. 284*, 325−335.
8. Hoogstraten, C. G., Legault, P., and Pardi, A. (1998) *J. Mol. Biol. 284*, 337−350.
9. Hoogstraten, C. G., Wank, J. R., and Pardi, A. (2000) *Biochemistry 39*, 9951−9958.
10. Feig, A. L., and Uhlenbeck, O. C. (1999) in *The RNA World* (Gesteland, R. F., Cech, T. R., and Atkins, J. F., Eds.) 2nd ed., pp 287−319, Cold Spring Harbor Laboratory Press, Plainview, NY.
11. van Tol, H., Buzayan, J. M., Feldstein, P. A., Eckstein, F., and Bruening, G. (1990) *Nucleic Acids Res. 18*, 1971−1975.
12. Glusker, J. P. (1991) in *Advances in Protein Chemistry* (Anfinsen, C. B., Edsall, J. T., Richards, F. M., and Eisenberg, D. S., Eds.) pp 1−76, Academic Press, Orlando, FL.
13. Westhof, E., and Hermann, T. (1999) *Nat. Struct. Biol. 6*, 208−209.
14. Wedekind, J. E., and McKay, D. B. (2000) *Methods Enzymol. 317*, 149−168.
15. Otwinowski, Z., and Minor, W. (1997) *Methods Enzymol. 276*, 307−326.
16. Brünger, A. T., Adams, P. D., Clore, G. M., DeLano, W. L., Gros, P., Grosse-Kunstleve, R. W., Jiang, J.-S., Kuszewski, J., Nilges, M., Pannu, N. S., Read, R. J., Rice, L. M., Simonson, T., and Warren, G. L. (1998) *Acta Crystallogr. D54*, 905−921.
17. Bailey, S. (1994) *Acta Crystallogr. D50*, 760−763.
18. Jones, A. (1978) *J. Appl. Crystallogr. 11*, 268−272.
19. Jones, T. A., Zhou, J. Y., Cowan, S. W., and Kjeldgaard, M. (1991) *Acta Crystallogr. A47*, 110−119.
20. Hingerty, B. E., Brown, R. S., and Klug, A. (1982) *Biochim. Biophys. Acta 697*, 78−82.
21. Shi, H., and Moore, P. B. (2000) *RNA 6*, 1091−1105.
22. Jovine, L., Djordjevic, S., and Rhodes, D. (2000) *J. Mol. Biol. 301*, 401−414.
23. Cate, J. H., and Doudna, J. A. (1996) *Structure 4*, 1221−1229.
24. Butcher, S. E., Allain, F. H., and Feigon, J. (2000) *Biochemistry 39*, 2174−2182.
25. Koizumi, M., and Ohtsuka, E. (1991) *Biochemistry 30*, 5145−5150.
26. Slim, G., and Gait, M. J. (1991) *Nucleic Acids Res. 19*, 1183−1188.
27. Rupert, P. B., and Ferre-D'Amare, A. R. (2001) *Nature 410*, 780−786.
28. Rupert, P. B., Massey, A. P., Sigurdsson, S. T., and Ferre-D'Amare, A. R. (2002) *Science 289*, 1421−1424.
29. Esnouf, R. M. (1997) *J. Mol. Graphics Modell. 15*, 133−138.

BI0300783